Research Article

Shina Daniel Oloniiju, Yusuf Olatunji Tijani*, and Olumuyiwa Otegbeye

Thermal analysis of extended surfaces using deep neural networks

https://doi.org/10.1515/phys-2024-0051
received March 08, 2024; accepted June 11, 2024

Abstract: The complexity of thermal analysis in practical systems has emerged as a subject of interest in various fields of science and engineering. Extended surfaces, commonly called fins, are crucial cooling and heating mechanisms in many applications, such as refrigerators and power plants. In this study, by using a deterministic approach, we discuss the thermal analysis of conduction, convection, and radiation in the presence of a magnetic force within an extended surface. The present study develops a deep neural network to analyze the mathematical model and to estimate the contributions of each dimensionless model parameter to the thermal dynamics of fins. The deep neural network used in this study makes use of a feedforward architecture in which the weights and biases are updated through backward propagation. The accuracy of the neural network model is validated using results obtained from a spectral-based linearization method. The efficiency rate of the extended surfaces is computed using the neural network and spectral methods. The results obtained demonstrate the accuracy of the neural network-based technique. The findings of this study in relation to the novel mathematical model reveal that utilizing materials with variable thermal conductivity enhances the efficiency rate of the extended surface.

Keywords: neural network approximation, spectral methods, fins, convection, conduction, magnetic

Nomenclature

a	cross-section area of the fin (m^2)
B_0	magnetic field intensity (T)
c_p	specific heat capacity (J/kg K)
F	temperature (K)
F_∞	temperature (ambient) (K)
g	acceleration due to gravity (m/s^2)
H	magnetic parameter
ι	internal heat generation (W/m^3)
J_e	conduction intensity
k	thermal conductivity (W/m K)
k_a	thermal conductivity (ambient)
K	permeability (m^2)
L	length of the fin (m)
M	thermo-geometric parameter
n	multi-boiling heat parameter
N_F	temperature ratio
N_P	porosity parameter
N_R	thermal radiation parameter
P	perimeter of the fin (m)
Q	heat generation parameter
u	velocity in the porous fin (m/s)
V	velocity vector (m/s)
w	width of the fin (m)
x	Cartesian coordinate
Z_r	fin efficiency rate
Greek symbols	
α_0, α_1	thermal coefficient (1/K)
β	thermal expansion coefficient (1/K)
η	heat transfer coefficient (W/m^2 K)
η_b	heat transfer coefficient (base)
ε	emissivity coefficient

*** Corresponding author: Yusuf Olatunji Tijani,** Department of Mathematics, Rhodes University, Makhanda, P.O. Box 94, Grahamstown 6140, South Africa, e-mail: yusuf.tijani@ru.ac.za
Shina Daniel Oloniiju: Department of Mathematics, Rhodes University, Makhanda, P.O. Box 94, Grahamstown 6140, South Africa, e-mail: s.oloniiju@ru.ac.za
Olumuyiwa Otegbeye: School of Computer Science and Applied Mathematics, University of Witwatersrand, Johannesburg, South Africa, e-mail: olumuyiwa.otegbeye@wits.ac.za

ρ	density of the fin (kg/m^3)
ν	kinematic viscosity (m^2/s)
ϕ_0, ϕ_1	temperature ratio
σ	electrical conductivity (S/m)
σ_*	Stefan-Boltzmann constant
ξ	thermal coefficient (1/K)
ξ_*	temperature ratio
ζ	dimensionless length
Γ	dimensionless temperature
Subscripts	
∞	ambient condition
w	reference (base)

1 Introduction

Understanding the behaviour of a system that is influenced by convective, magnetic, and radiative heat transfer conditions is a long-standing and crucial aspect in the field of thermal transport. This subject has considerable significance in various industries, including aerospace, construction, energy, and manufacturing, thus underscoring its broad and practical utility. One example of such a system is the fin. The relevance of fins is evident in our daily lives, influencing cooling processes in refrigerators, the radiator systems in cars, the heating elements in geysers, the thermal fins used in heat dissipation in our computers, and numerous other applications around us. In these applications, fins are crucial to enhancing heat transfer, improving efficiency, and preventing overheating. Fins, or extended surfaces, improve heat transfer efficiency from surfaces that typically undergo cooling via natural or forced convection by gases or fluids. Heat is conducted from the heat source to the fin's surface through thermal conduction. Heat is usually transferred by radiation, convection, and conduction. On the other hand, heat from the surrounding medium, the magnetic element, and the material porosity can all contribute to thermal dissipation. Fins have three fundamental characteristics: (i) they are metallic; (ii) they have a variety of structures; and (iii) the fin's length is significantly longer than its diameter [1].

The mechanisms of fins have been the subject of numerous investigations; one noteworthy study is by Gorla and Bakier [2], which examined heat dissipation due to radiation and conduction in a rectangular porous fin. The study used the Darcy model to simplify the momentum equation. The fin system studied by Gorla and Bakier [2] takes into account conduction and radiation-induced thermal equilibrium while ignoring internal heat generation and the role of magnetic fields in heat enhancement. The significance of porosity in fins in a parallel-surface channel was studied by Kiwan and Al-Nimr [3]. Numerical analyses of the heat enhancement resulting from a porous fin were carried out in the study. A 100% decrease in the fin material's weight was noted, and it was concluded that the fin material has the same performance as a solid fin. The effect of the thickness of a porous fin on the thermal system was examined in the study. Hatami and Ganji [4] investigated the effect of geometrical and material properties in the design of porous fins using the least squares approach. The results show that fins made of aluminum have a high rate of heat transmission, which makes them appropriate for extended surface design. Gireesha *et al.* [5] investigated the effects of stretching and shrinking on the temperature distribution of a wet longitudinal fin. According to the analysis, the negative impacts of motion and internal heat generation on the fin's heat transfer rate can be lessened by putting in place a shrinking mechanism on the extended surface. Other studies in this direction include the work of Atouei *et al.* [6], Nicholls *et al.* [7], Aziz and Lopez [8], Razani and Ahmadi [9], Buonomo *et al.* [10], and the references therein.

Research into extended surfaces has made a substantial contribution to understanding the accuracy and efficiency of semi-analytical and numerical discretization methods. These studies are motivated by the complex dynamical equation (a second-order nonlinear ordinary differential equation) that governs heat transfer in extended surfaces. These equations often do not have simple closed-form solutions, especially when they are nonlinear. For instance, Aderogba *et al.* [11] used the generalized fins model to evaluate the performance of the nonstandard finite difference numerical discretization technique. It was demonstrated that the numerical approach maintained the dynamics of the differential equation with good accuracy. The hybridization of the differential transform and Pade approximation method was used by Sowmya *et al.* [12] to investigate heat transfer in rectangular fins under the influence of a magnetic field. Kasali *et al.* [13] used the spectral-based local linearization method introduced by Motsa [14] to investigate the effects of the multi-boiling parameter on linear and nonlinear thermal conductivity on thermal flux on an extended surface. The study also assessed the accuracy of the spectral-based method. Akindeinde [15] investigated the efficiency and accuracy of the Parker-Sochacki semi-analytical method using the dynamical nonlinear fin model as a case study. Sobamowo [16] studied porous wet fins subjected to magnetic body forces and thermal radiation using the conventional finite difference approach. To predict heat dissipation in an extended surface subjected to conductive, convective, and radiative conditions, Zhanga and Li [17] presented a novel Taylor approximate approach. The study evaluated the accuracy of the method by contrasting their approach

with explicit solutions in limiting cases, such as those without a radiation effect. Roy *et al.* [18] examined the model of an accelerating triangular fin and the performance of a modified decomposition method.

Machine learning has revolutionized various fields, including computer vision, natural language processing, and speech recognition, among many others. Recently, researchers have focused on training computer systems to process data and information in a manner similar to the human brain. This technique, known as the neural networks method, is a part of a broader category of machine learning processes called deep learning. Lagaris *et al.* [19] initially proposed solving an ordinary differential equation using neural networks. The underlying principle involves training a neural network framework to meet the conditions stipulated by a differential equation. Waseem *et al.* [20] analyzed the temperature distribution in a porous fin through artificial neural networks coupled with the cuckoo algorithm. Tan *et al.* [21] used the neural network method to analyze heat efficiency in a compact exchanger. Goud *et al.* [22] used a Levenberg-Marquardt neural network technique to study heat transfer in a trapezoidal-shaped fin. They took into account assumptions on heat conductivity that depart from traditional Fourier principles. Kumar *et al.* [23] investigated the heat efficiency mechanism in a wavy wall with an artificial neural network. Shafiq *et al.* [24] used the artificial neural network method to estimate key parameters related to engineering physical quantities in a bioconvection nanofluid flow over a stretching surface containing gyrotactic microorganisms. In other related studies, Shafiq *et al.* [25] used artificial neural networks to forecast the potential number of deaths from the COVID-19 pandemic in Italy. In addition, Shafiq *et al.* [26] investigated the effects of Soret and Dufour convective heat transfer using an accelerating needle as the focal point, with the simulations conducted through artificial neural networks.

Notably, none of the many studies published in the literature have examined the application of deep learning methods to the analysis of heat dissipation and temperature distribution in a rectangular porous fin subjected to radiation, magnetic effects, and quadratic-type thermal conductivity. To this end, this study examines heat dissipation in a porous extended surface (fin) exposed to radiation, convection, and conductivity in a magnetic environment. The dynamical system is analyzed using a deep neural network (DNN) and the physical implications of the findings are reported. The spectral-based local linearization method, introduced by Motsa [14], is used to validate the accuracy of the result obtained using the deep learning approach.

2 Analysis of the mathematical model

This section begins by developing the mathematical model. In the context of a porous fin, the following dynamical cumulative heat addition equation describes the equilibrium of thermal transport [13,27]:

$$z(x) = z(x + \delta x) + z_{\text{conv}} + z_{\text{rad}} + z_{\text{mag}} + z_{\text{int}} + \text{porous term}. \tag{1}$$

Eq. (1) represents the thermal energy balance within a closed system. Heat conduction into the base of the fin element at position x is the sum of heat conduction into the element at the fin tip $(x + \delta x)$, heat convection from the element, heat radiation from the element, heat transfer due to the magnetic field, internal heat generation within the element, and the contribution from the porous term. The porous media is homogeneous and saturates with a single-phase fluid. The study focuses on a convective-conductive-radiative porous fin with length L. The fin is exposed on both faces to convection with a temperature F_∞ and subjected to a uniform magnetic field, as illustrated in Figure 1. The longitudinal fin is constrained in length with an insulated tip, creating an adiabatic system where no heat is transmitted from the tip. The temperature at the base of the fin is denoted as $F = F_w$ and at the tip takes the form of a Neumann boundary condition, $\frac{\mathrm{d}F}{\mathrm{d}x} = 0$. The interaction between the porous medium and the single-phase fluid is formulated using the Darcy model. Body force due to the magnetic field is experienced in the y-direction. It is assumed that the radiative heat flux behaves similarly to an optically thick gas within the porous medium. The effect

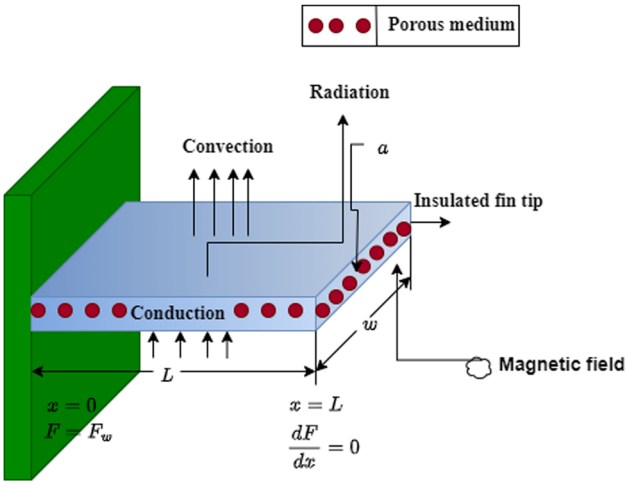

Figure 1: Geometrical configuration of the fin.

of the electrical field due to polarization is considered to be negligible, i.e., $E = 0$. If this phenomenon takes place in a steady-state condition, then Eq. (1) becomes [13]:

$$\left.\begin{aligned} z(x) - z(x+\delta x) = {} & \underbrace{\eta(F)(F-F_\infty)\delta a}_{\text{heat due to convection}} + \underbrace{\varepsilon\sigma_*(F^4-F_\infty^4)\delta a}_{\text{heat due to radiation}} \\ & + \underbrace{\frac{J_e \times J_e}{\sigma} a\delta x}_{\text{heat due to magnetic element}} + \underbrace{z_{\text{int}}(F)a\delta x}_{\text{internal heat dissipation}} \\ & + \underbrace{\rho c_p w u(x)(F-F_\infty)\delta x}_{\text{heat due to porous effect}} \end{aligned}\right\}. \tag{2}$$

Here, $u(x)$ represents the movement of the buoyancy-driven flow at any location x, and J_e is the intensity of the conduction responsible for the thermal transport due to electric current, given, respectively, as [1]

$$u(x) = \frac{g\beta K}{\nu}(F - F_\infty), \quad \text{and} \quad J_e = \sigma(E + V \times B). \tag{3}$$

By substituting Eq. (3) into Eq. (2), we obtain

$$\left.\begin{aligned} z(x) - \left(z(x) + \frac{\mathrm{d}z}{\mathrm{d}x}\delta x\right) = {} & \eta(F)(F-F_\infty)P\delta x \\ & + \varepsilon\sigma_*(F^4 - F_\infty^4)P\delta x \\ & + \frac{J_e \times J_e}{\sigma} a\delta x + z_{\text{int}}(F)a\delta x + \frac{\rho c_p g\beta K}{\nu} w(F-F_\infty)^2\delta x, \end{aligned}\right\} \tag{4}$$

where $\delta a = P\delta x$.

According to Ohm's law, the current density or conduction intensity is obtained as $J_e = \sigma(E + V \times B)$, where E denotes the electric field, V is the charge carrier velocity, which is accounted for using the model $u = \frac{g\beta K}{\nu}(F - F_\infty)$, since porosity is considered, σ is the electrical conductivity, and B is the magnetic force. Thus, if the electric field is negligible, that is, $E = 0$; we have

$$J_e = \sigma(V \times B). \tag{5}$$

Here, $V = (u, v)$, Eq. (5) indicates that $J_e = \sigma|u||B|\sin\theta\hat{n}$, and thus,

$$J_e \times J_e = \sigma|u||B_0|\sin\theta\hat{n} \times \sigma|u||B_0|\sin\theta\hat{m} = \sigma^2u^2B_0^2\sin^2\theta. \tag{6}$$

Note that the velocity of the charged particle is perpendicular to the magnetic field, and thus, $\sin^2\theta = 1$. Hence [1],

$$\frac{J_e \times J_e}{\sigma} = \sigma u^2 B_0^2. \tag{7}$$

Upon division by δx, Eq. (4) reduces to

$$\begin{aligned} -\frac{\mathrm{d}z}{\mathrm{d}x} = {} & \eta(F)P(F-F_\infty) + \varepsilon\sigma_*P(F^4 - F_s^4) \\ & + a\sigma B_0^2 u(x)^2 + az_{\text{int}}(F) + \frac{\rho c_p g\beta K}{\nu} w(F-F_\infty)^2, \end{aligned} \tag{8}$$

where $\frac{J_e \times J_e}{\sigma} = \sigma B_0^2 u(x)^2$. Following Fourier's law of heat conduction [28], heat conduction taking place within the fin can be mathematically described as [4]:

$$z = -ak(F)\frac{\mathrm{d}F}{\mathrm{d}x}. \tag{9}$$

Substituting Eq. (9) into Eq. (8), we have

$$\left.\begin{aligned} \frac{\mathrm{d}}{\mathrm{d}x}\left(ak(F)\frac{\mathrm{d}F}{\mathrm{d}x}\right) = {} & \eta(F)P(F-F_\infty) + \varepsilon\sigma_*P(F^4 - F_\infty^4) \\ & + a\sigma\frac{B_0^2 g^2\beta^2K^2}{\nu^2}(F-F_\infty)^2 + az_{\text{int}}(F) \\ & + \frac{\rho c_p g\beta K}{\nu} w(F-F_\infty)^2, \end{aligned}\right\} \tag{10}$$

and using the relation given in Singha *et al.* [29], Oguntala and Abd-Alhameed [30], and Sobamowo *et al.* [31], we have

$$\left.\begin{aligned} k(F) &= k_a[1 + \alpha_0(F-F_\infty) + \alpha_1^2(F-F_\infty)^2], \\ \eta(F) &= \eta_b\left(\frac{F-F_\infty}{F_w - F_\infty}\right)^n, \\ \text{and} \quad z_{\text{int}}(F) &= \iota[1 + \xi(F-F_\infty)]. \end{aligned}\right\} \tag{11}$$

After some simplifications, Eq. (10) becomes

$$\left.\begin{aligned} & \frac{\mathrm{d}}{\mathrm{d}x}\left[k_a[1 + \alpha_0(F-F_\infty) + \alpha_1^2(F-F_\infty)^2]\frac{\mathrm{d}F}{\mathrm{d}x}\right] \\ & - \frac{\eta_b P(F-F_\infty)^{n+1}}{a(F_w - F_\infty)^n} - \frac{\varepsilon\sigma_*P}{a}(F^4 - F_\infty^4) \\ & - \iota[1 + \xi(F-F_\infty)] - \frac{\sigma B_0^2 g^2\beta^2K^2}{\nu^2}(F-F_\infty)^2 \\ & - \frac{\rho c_p g\beta K w}{a}(F-F_\infty)^2 = 0, \end{aligned}\right\} \tag{12}$$

with associated boundary conditions given as [2]:

$$\left.\begin{aligned} &\text{at} \quad x = 0, \quad F = F_w, \\ &\text{at} \quad x = L, \quad \frac{\mathrm{d}F}{\mathrm{d}x} = 0. \end{aligned}\right\} \tag{13}$$

We further introduce the following dimensionless variables and parameters:

$$\left.\begin{aligned}
&\zeta = \frac{x}{L}, \quad \Gamma = \frac{F - F_\infty}{F_w - F_\infty}, \quad M = \frac{\eta_b P L^2}{a k_a},\\
&Q = \frac{\iota L^2}{k_a(F_w - F_\infty)}, \quad \phi_0 = \alpha_0(F_w - F_\infty),\\
&\phi_1 = \alpha_1^2(F_w - F_\infty)^2, \quad N_P = \frac{\rho c_p g \beta K w L^2 (F_w - F_\infty)}{a \nu k_a},\\
&N_R = \frac{L^2 \sigma_* P (F_w - F_\infty)^3}{a k_a},\\
&N_F = \frac{F_\infty}{F_w - F_\infty}, \quad \xi_* = \xi(F_w - F_\infty),\\
&H = \frac{\sigma B_0^2 g^2 \beta^2 K^2 L^2 (F_w - F_\infty)}{\nu^2 k_a}.
\end{aligned}\right\} \tag{14}$$

By incorporating the nondimensional variable in Eq. (14) into Eqs (12) and (13), we obtain the following single variable differential equation:

$$\begin{aligned}
&\frac{\mathrm{d}}{\mathrm{d}\zeta}\left[K_1(\Gamma)\frac{\mathrm{d}\Gamma}{\mathrm{d}\zeta}\right] - M\Gamma^{n+1} - \varepsilon N_R[(N_F + \Gamma)^4 - N_F^4]\\
&\quad - (H + N_P)\Gamma^2 - Q(1 + \xi_*\Gamma) = 0,
\end{aligned} \tag{15}$$

where $K_1(\Gamma) = 1 + \phi_0\Gamma + \phi_1\Gamma^2$ and its associated insulated boundary conditions [2]

$$\text{at} \quad \zeta = 0, \ \Gamma = 1, \quad \text{and} \quad \text{at} \ \zeta = 1, \ \frac{\mathrm{d}\Gamma}{\mathrm{d}\zeta} = 0. \tag{16}$$

2.1 The fin efficiency rate

The fin efficiency is computed by dividing the rate of heat transfer (Z_{fin}) by the ideal rate of heat transfer (Z_{ideal}), where the latter represents the thermal energy that would be conducted if the entire fin temperature were the same as the temperature of the fin base. This relationship is expressed as follows [1]:

$$Z_r = \frac{Z_{\text{fin}}}{Z_{\text{ideal}}} = \frac{\int_0^L P(F - F_\infty)\mathrm{d}x}{PL(F_w - F_\infty)} = \int_0^1 \Gamma(\zeta)\mathrm{d}\zeta, \tag{17}$$

where $Z_{\text{fin}} = \int_0^L P(F - F_\infty)\mathrm{d}x$ is the rate of heat transfer.

3 Method of solution

In this section, we introduce the implementation of a DNN to solve Eq. (15) subject to the associated boundary conditions (16). Subsequently, we derive the algorithm and describe the implementation of the spectral local linearization method (SLLM) to solve the differential equation.

3.1 DNNs approximation of the model solution

This study uses a deep and fully connected feedforward artificial neural networks framework to solve the nonlinear differential Eq. (15) with the associated boundary conditions (16). Suppose the differential Eq. (15) is defined as follows:

$$\mathcal{G}\left[\zeta, \Gamma(\zeta), \frac{\mathrm{d}\Gamma(\zeta)}{\mathrm{d}\zeta}, \frac{\mathrm{d}^2\Gamma(\zeta)}{\mathrm{d}\zeta^2}\right] = 0, \quad \zeta \in [0, 1], \tag{18}$$

subject to the conditions in Eq. (16), where $\mathcal{G}$ is a nonlinear operator of $\Gamma(\zeta)$ and its derivatives. The collocation technique is used to discretize the domain and boundary of the problem into a finite number of discrete points. In this study, we use the set of Chebyshev-Gauss-Lobatto points,

$$\tilde{\zeta}_j = -\cos\left(\frac{\pi j}{M_\zeta}\right), \quad j = 0, \ldots, M_\zeta,$$

mapped onto $\zeta \in [0, 1]$ through the linear mapping, $\zeta = \frac{1}{2}(\tilde{\zeta} + 1)$. The nonlinear differential Eq. (18) is then transformed into its discrete equivalent

$$\begin{aligned}
&\mathcal{G}\left[\zeta_j, \Gamma(\zeta_j), \frac{\mathrm{d}\Gamma(\zeta_j)}{\mathrm{d}\zeta}, \frac{\mathrm{d}^2\Gamma(\zeta_j)}{\mathrm{d}\zeta^2}\right] = 0,\\
&\qquad \zeta_j \in \frac{1}{2}(\tilde{\zeta} + 1) \equiv [0, 1],
\end{aligned} \tag{19}$$

subject to the conditions

$$\Gamma(\zeta_0) = 1 \quad \text{and} \quad \frac{\mathrm{d}\Gamma(\zeta_{M_\zeta})}{\mathrm{d}\zeta} = 0. \tag{20}$$

In this study, we consider the ansatz, $\Gamma_t(\zeta; w, b)$, which satisfies the boundary conditions (20) for the solution of the differential Eq. (19). Here, w and b are the weights and biases, respectively, of the DNNs framework. Therefore, the problem of approximating the solution of the differential equation then becomes the unconstrained minimization problem,

$$\min_{w,b} \sum_{\zeta_j \in [0,1]} \left\{\mathcal{G}\left[\zeta_j, \Gamma_t(\zeta_j; w, b), \frac{\mathrm{d}\Gamma_t(\zeta_j; w, b)}{\mathrm{d}\zeta}, \frac{\mathrm{d}^2\Gamma_t(\zeta_j; w, b)}{\mathrm{d}\zeta^2}\right]\right\}^2. \tag{21}$$

In the proposed technique, the trial solution, $\Gamma_t(\zeta; w, b)$, is defined as follows:

$$\begin{aligned}
\Gamma_t(\zeta; w, b) = 1 + \zeta\Bigg(&N(\zeta; w, b) - N(1; w, b)\\
&- \frac{\mathrm{d}N(1; w, b)}{\mathrm{d}\zeta}\Bigg).
\end{aligned} \tag{22}$$

The trial solution, $\Gamma_t(\zeta; w, b)$, depends on the output, $N(\zeta; w, b)$, of the neural networks framework and is chosen to satisfy the boundary conditions, (16), of the differential

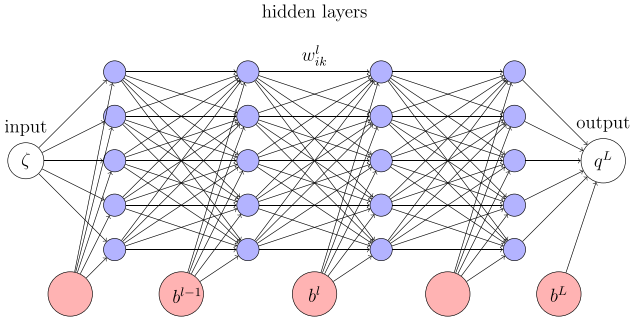

Figure 2: Schematic diagram of a fully connected DNN.

model. $N(\zeta;\, w, b)$ is the single output of a feedforward DNN architecture fed with a single input vector, ζ_j, with parameters, w and b, which are the weights and biases of the neural network architecture.

The neural network architecture is a $L + 1$ fully connected layers, as shown in Figure 2, which consist of the first layer, which is the input through which the input vector ζ_j is fed, the last layer, which is the output layer and $L - 1$ hidden layers. Activation functions are introduced in the hidden layers to introduce nonlinearity to the neural network architecture. In this study, the sigmoid activation function, $\varrho(q) = (1 + e^{-q})^{-1}$, is used; however, other functions such as the hyperbolic tangent, rectified linear units and exponential functions can be used. Each neuron in each hidden layer and the output layer has a bias, and the neurons in layers $l - 1$ and l are connected by the weights. The weights which connect neuron k in layer $l - 1$ to neuron i in the lth layer are represented by w^l_{ik}, and the bias associated with neuron i in layer l is denoted by b^l_i.

The neural network framework is expressed mathematically as follows:

$$\left.\begin{aligned} q^0 &= \zeta, && \text{the input layer} \\ q^l &= \varrho^l(w^l q^{l-1} + b^l),\ 1 < l < L - 1, && \text{the hidden layers} \\ q^L &= w^L q^{L-1} + b^L, && \text{the output layer}, \end{aligned}\right\} \tag{23}$$

where the result of the output layer, $q^L = N(\zeta;\, w, b)$, is used in the trial solution (22). To find the weights and biases in the layers, we minimize the residual function

$$\mathcal{R}(w, b) = \sum_{j=0}^{M_\zeta} \left[\mathcal{G}\left[\zeta_j, \Gamma_t(\zeta_j;\, w, b), \frac{\mathrm{d}\Gamma_t(\zeta_j;\, w, b)}{\mathrm{d}\zeta}, \frac{\mathrm{d}^2\Gamma_t(\zeta_j;\, w, b)}{\mathrm{d}\zeta^2} \right] \right]^2, \tag{24}$$

using gradient descent optimization with adaptive moment estimation. Lagaris *et al.* [19] showed how to obtain the automatic partial derivatives of the residual function with respect to the weights and biases. However, in this study, we used the GradientTape sub-module of Python's TensorFlow package. The weights and biases are then updated through backward propagation. The neural network is completely implemented with Python programming language using the TensorFlow and NumPy packages. The algorithm for the neural networks approximation of the solution of Eq. (15) is given in Algorithm 1. Figure 3 shows the training loss curve of the neural network architecture. The figure depicts the plot of the value of the loss function (24) against the number of training or epochs. The loss function measures how well the trial function (22), which is dependent on the neural network framework (23), approximates the solution of the differential Eq. (15). During the training process, the network adjusts its parameters, *viz.* weights and biases, iteratively to minimize the loss and improve the predictability of the trial solution as an approximate solution of Eq. (15). We note here that the weights and biases are initialized using normal distributions centred at zero with standard deviations of 0.5.

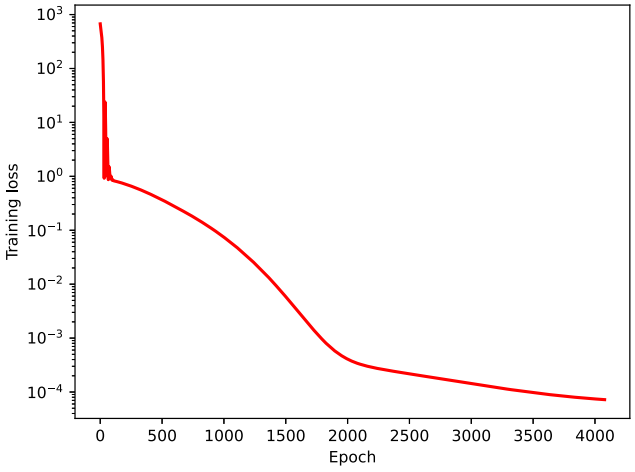

Figure 3: Training loss curve of the neural networks algorithm with 6 hidden layers and 50 neurons in each hidden layer.

Algorithm 1. Step-by-step algorithm for solving Eq. (15) using a fully connected deep neural network.

procedure DNN APPROXIMATION OF THE SOLUTION OF Eq. (15)
Define the variable $q^0 = \zeta$ as input.
Define the number of hidden layers and number of neurons in each layer.
Initialize the weights and biases for each layer and set them as trainable parameters.
Define the neural networks architecture:
for $l = 1$ **to** L **do**
    $q^l = \varrho^l(w^l q^{l-1} + b^l)$
end for

9: Define the trial solution: $\Gamma_t(\zeta; w, b) = 1 + \zeta(N(\zeta; w, b) - N(1; w, b) - N'(1; w, b))$.
10: Define the loss function $\mathcal{R}(w, b)$ in Eq. (24) in terms of the trial function.
11: Define the model parameters, ϕ_0, ϕ_1, M, n, ε, N_R, N_F, H, N_P, Q, ξ_* as untrainable parameters.
12: Train the neural network model to optimize the weights and biases by minimizing the residual function.
13: **end procedure**

3.2 Spectral local linearization method

In this section, we implement the SLLM to approximate the solution of Eq. (15) subject to the associated boundary conditions (16). Taking $n = 1$ and applying a first-order Taylor series expansion around an initial guess of the solution of the differential equation, we obtain a linearized form of the equation expressed concisely as follows:

$$[a_{1,r}]\Gamma''_{r+1} + [a_{2,r}]\Gamma'_{r+1} + [a_{3,r}]\Gamma_{r+1} = a_{4,r}, \tag{25}$$

where r and $r + 1$ represent two successive iterations, and the coefficients are defined as follows:

$$\left.\begin{aligned} a_{1,r} &= 1 + \phi_0\Gamma_r, \quad a_{2,r} = 2\phi_0\Gamma'_r + 3\phi_1\Gamma'^2_r, \\ a_{3,r} &= \phi_0\Gamma''_r - 2M\Gamma_r - 4\varepsilon N_R N_F^3 - 12\varepsilon N_R N_F^2\Gamma_r \\ &\quad - 12\varepsilon N_R N_F\Gamma_r^2 - 4\varepsilon N_R\Gamma_r^3 - 2(1 + N_P) - Q\xi_*, \\ a_{4,r} &= \phi_0\Gamma'^2_r + 2\phi_1\Gamma'^3_r + \phi_0\Gamma_r\Gamma''_r - M\Gamma_r^2 - 6\varepsilon N_R N_F^2\Gamma_r^2 \\ &\quad - 8\varepsilon N_R N_F\Gamma_r^3 - 3\varepsilon N_R\Gamma_r^4 - (H + N_P)\Gamma_r^2 + Q. \end{aligned}\right\} \tag{26}$$

For the sake of brevity, prime $'$ denotes differentiation of Γ with respect to ζ, that is, $\Gamma' = \frac{d\Gamma}{d\zeta}$, $\Gamma'' = \frac{d^2\Gamma}{d\zeta^2}$. The boundary conditions are expressed as follows:

$$\Gamma(\zeta = 0)_{r+1} = 1, \quad \Gamma'(\zeta = 1)_{r+1} = 0. \tag{27}$$

The linearized Eq. (25) and the boundary condition (27) are discretized using the Chebyshev pseudospectral method on the Chebyshev-Gauss-Lobatto nodes. We refer the readers to Trefethen [32] for a full description and implementation of this numerical method. Following Trefethen [32], the implementation of the pseudospectral method on Eq. (25) results in the following equation

$$[[\mathbf{a}_{1,r,i}]\boldsymbol{D}^2 + [\mathbf{a}_{2,r,i}]\boldsymbol{D} + [\mathbf{a}_{3,r,i}]\mathbf{I}]\boldsymbol{\Gamma}_{r+1,i} = \mathbf{a}_{4,r,i}, \tag{28}$$

where $\mathbf{I}$ is an identity matrix of dimension $(M_\zeta + 1) \times (M_\zeta + 1)$, ($M_\zeta$ is the number of collocation points), $\mathbf{D}$ is a scaled differentiation matrix [32], and $\boldsymbol{\Gamma}$ is the unknown vector solution. Eq. (27) is discretized as follows:

$$\Gamma_{r+1,0} = 1, \quad \mathbf{D}\Gamma_{r+1,M_\zeta} = 0. \tag{29}$$

Eq. (28) can then be concisely expressed as follows:

$$\mathbf{A}\boldsymbol{\Gamma}_{r+1,i} = \mathbf{a}_{4,r,i}, \tag{30}$$

where

$$\mathbf{A} = [\mathbf{a}_{1,r,i}]\boldsymbol{D}^2 + [\mathbf{a}_{2,r,i}]\boldsymbol{D} + [\mathbf{a}_{3,r,i}]\mathbf{I},$$

which together with the imposition of the boundary conditions (29) results in the following consistent matrix-vector system

$$\begin{bmatrix} 1 & 0 & \cdots & \cdots & 0 & 0 \\ \multicolumn{6}{c}{\mathbf{A}} \\ D_{M_\zeta,0} & D_{M_\zeta,1} & \cdots & \cdots & D_{M_\zeta,M_\zeta-1} & D_{M_\zeta,M_\zeta} \end{bmatrix} \begin{bmatrix} \Gamma_{r+1,0} \\ \Gamma_{r+1,1} \\ \vdots \\ \Gamma_{r+1,M_\zeta-1} \\ \Gamma_{r+1,M_\zeta} \end{bmatrix} = \begin{bmatrix} 1 \\ a_{4,r,1} \\ \vdots \\ a_{4,r,M_\zeta-1} \\ 0 \end{bmatrix}. \tag{31}$$

4 Results and discussion

Insights into the thermal dynamics of extended surfaces are provided through parametric analysis of some key parameters in Eq. (15) using the DNN method. A comparison of the results obtained by DNN and SLLM is made to validate the results. If not specified otherwise, the analysis of the results was carried out using the following parameter values: $M = 1.0$, $N_R = 0.10$, $N_F = 0.10$, $n = 1.0$, $\varepsilon = 1.0$, $\phi_0 = 0.10$, $\phi_1 = 0.30$, $N_P = 1.0$, $H = 1.0$, $Q = 0.2$, and $\xi_* = 1.0$. The figures presented in this section depict the output obtained from using the DNN to learn the mathematical model in Eq. (15) with its conditions given in Eq. (16).

Figure 4 depicts the effect of linear and nonlinear thermal conductivity variations on the dynamics of the extended surface. Specifically, the figure illustrates how temperature distribution along the surface is influenced by the variations in the linearity and nonlinearity of the thermal conductivity. The distinction between linear and nonlinear thermal conductivity variations is significant for temperature distribution along extended surfaces. The linear relationship suggests that the thermal conductivity

of the fin changes uniformly with temperature. On the other hand, the nonlinear thermal conductivity variation has a much more complex, nonuniform or even nonmonotonic relationship with the temperature. It is apparent from Figure 4 that the linear variation of thermal conductivity results in a more uniform temperature distribution, particularly in the vicinity of the fin's base. This uniform temperature distribution at the fin's base can be attributed to the consistent and predictable changes in thermal conductivity along the surface. In contrast, the nonlinear variation introduces deviations in temperature distribution along the surface, leading to nonuniform temperature profiles. This nonuniformity may arise due to nonlinear effects such as phase transitions, variations in the material property of the fin or localized heat sources, which can disrupt the thermal equilibrium along the surface and lead to nonuniform temperature profiles, which may sometimes be necessary for the design of fins. Regardless of whether thermal conductivity variations are linear or nonlinear, the overall trend in temperature distribution remains consistent: as both parameters increase, the absolute temperature along the extended surface increases. This is because higher thermal conductivity values enable more efficient heat transfer, leading to higher temperatures along the surface.

The impact of both radiation and internal heat generation on the temperature of the fin are shown in Figure 5. Increasing the thermal radiation parameter reduces the temperature observed on the extended surface. This phenomenon arises because enhanced thermal radiation facilitates heat transfer away from the surface. A significant

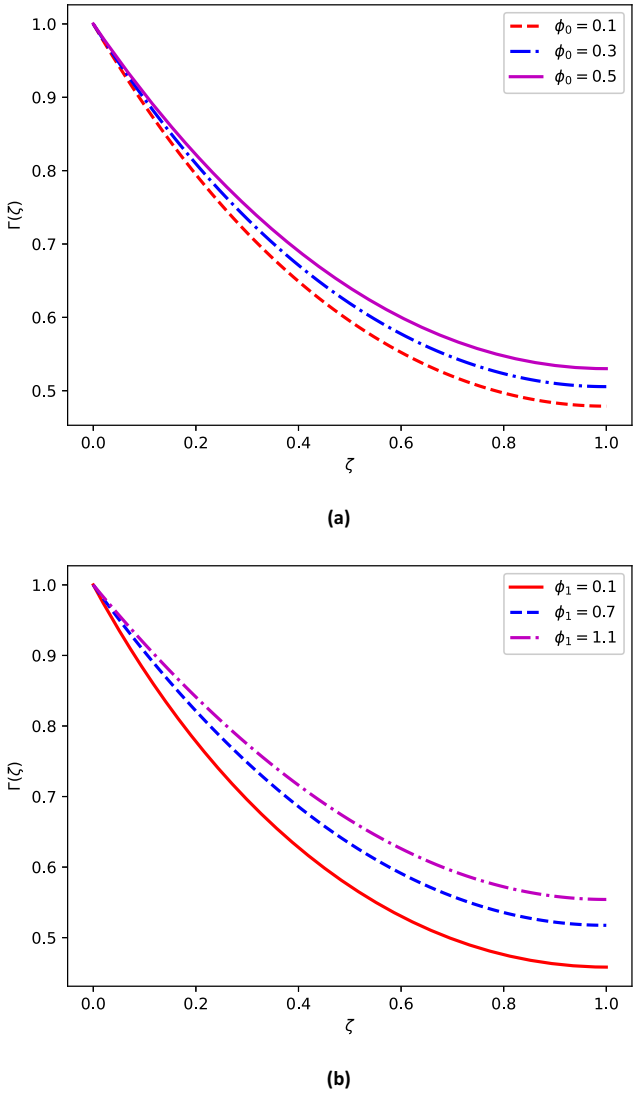

Figure 4: Effect of (a) linear, ϕ_0, (b) nonlinear, ϕ_1 thermal conductivity on temperature distribution on the fin.

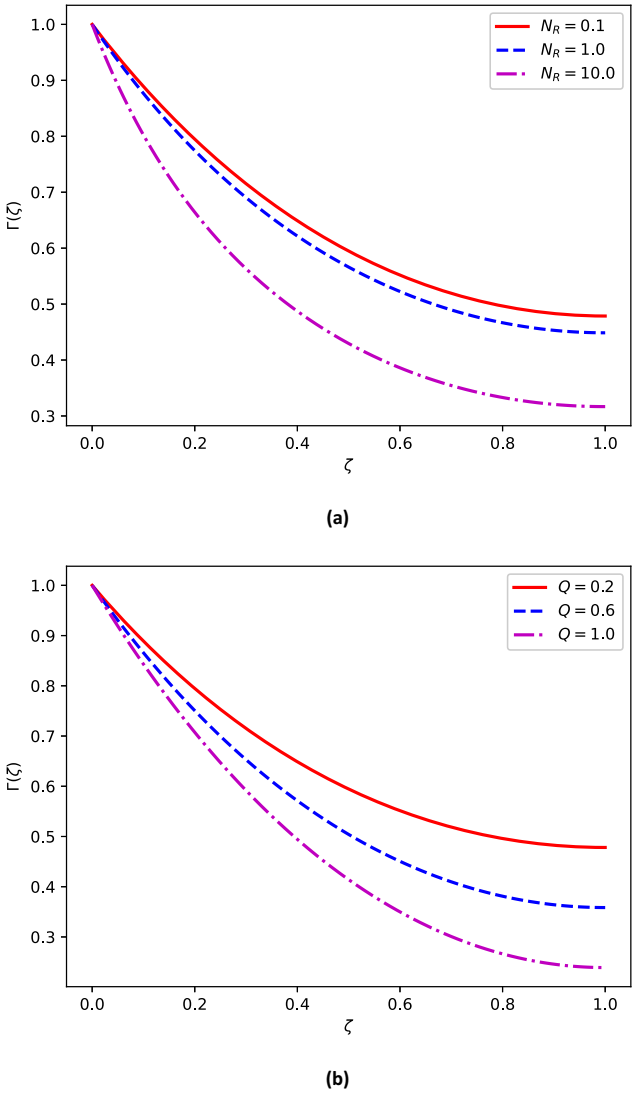

Figure 5: Effect of (a) radiation parameter, N_R, and (b) heat generation parameter, Q on the temperature distribution of the extended surface.

decrease in the temperature of the fin at its tip is experienced as the fin generates more internal heat. The increased internal heat generation parameter leads to a higher temperature change at the tip of the extended surface. This significant temperature gradient on the fin causes heat to be transferred more rapidly from the base of the fin to the tip. Consequently, the higher the value of the heat generation parameter, the lesser the temperature value at the tip of the extended surface since heat is effectively conducted and convected away from that region.

Figure 6 shows the effect of the multi-boiling and magnetic field strength parameters on the fin. The choice of the values of the multi-boiling parameters delineates distinct heat transfer regimes occurring on the extended surface. By varying this parameter, we can simulate and analyze the heat transfer behaviour under different boiling conditions, providing insights into the dynamics and thermal performance of the extended surface. When $n = -\frac{1}{4}$, it indicates laminar film boiling, where a thin film of vapour forms and envelops the fin surface. The temperature distribution in this regime is relatively low due to the insulating effect of the vapour film. On the other hand, $n = \frac{1}{4}$ corresponds to natural convection, where heat transfer occurs primarily through fluid motion driven by density variations caused by temperature gradients. Finally, $n = 2$ represents nucleate boiling, where discrete vapour bubbles form on the extended surface and detach to facilitate heat transfer. This regime is associated with high heat transfer coefficients due to the effective heat removal by vaporization and bubble motion as captured in Figure 6. Increasing the magnetic field parameter has a notable effect on the temperature distribution at the tip of the extended surface. As the parametric value of the magnetic field parameter increases, the temperature at the tip decreases. This dynamic is primarily driven by the amplified influence of the magnetic field due to a rise in the Hartman number. The Hartman number characterizes the ratio of magnetic force to viscous force and measures the strength of the magnetic field relative to fluid motion. An intensified magnetic field exerts a damping effect on the convective heat transfer process. Essentially, the magnetic field inhibits the movement of fluid particles, reducing their ability to carry heat away from the surface efficiently. Consequently, as the magnetic field becomes stronger, the convective heat transfer rate decreases, reducing overall heat transfer on the extended surface.

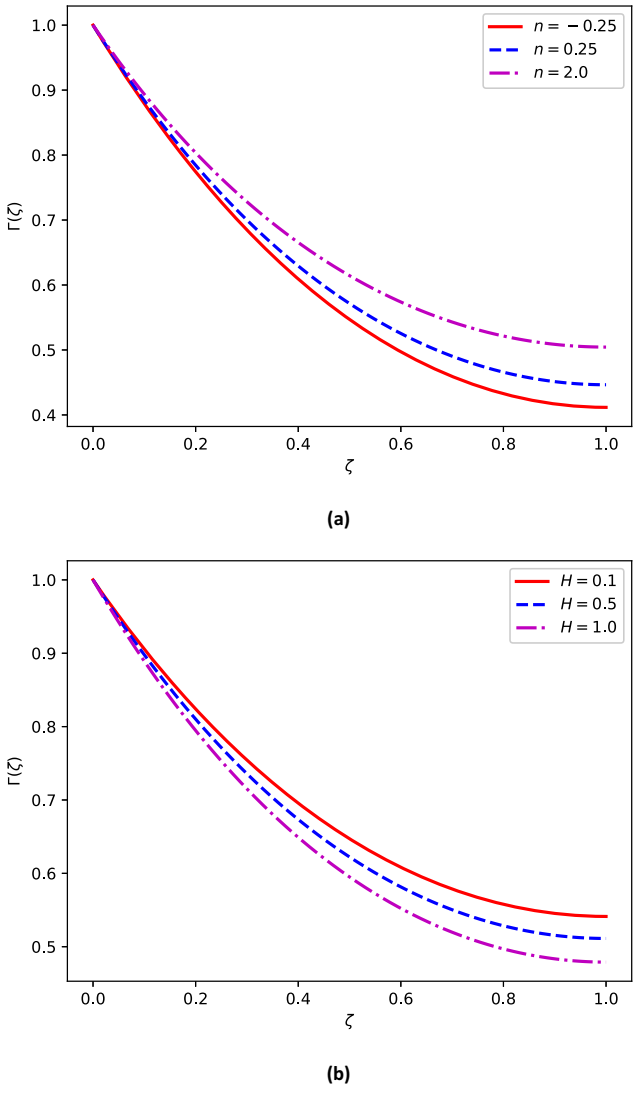

Figure 6: Effect of (a) multi-boiling, n, and (b) magnetic field strength, H, parameters on the fin's temperature distribution.

The efficiency rate of the extended surface, as evaluated using both the DNN approach and spectral-based

Table 1: The fin efficiency rate as computed using the DNN approach and the SLLM with the following values: $N_R = 0.10$, $n = 1.0$, $N_F = 0.10$, and $\xi_* = 0.6$

M	H	N_P	ϕ_0	ϕ_1	Q	DNN	SLLM
1.0	0.5	2.0	0	0	0	0.62475	0.62495
2.0	—	—	—	—	—	0.58602	0.58633
1.0	0.1	2.0	0	0	0	0.64334	0.64352
—	0.3	—	—	—	—	0.63385	0.63397
1.0	0.5	1.0	0	0	0	0.67598	0.67612
—	—	1.5	—	—	—	0.64839	0.64852
1.0	0.5	1.0	0.1	0.3	0.6	0.62901	0.62930
—	—	—	0.3	—	—	0.65383	0.65391
1.0	0.5	1.0	0.3	0.1	0.6	0.63411	0.63418
—	—	—	—	0.7	—	0.68814	0.68849
1.0	0.5	1.0	0.3	0.3	0.4	0.68096	0.68118
—	—	—	—	—	1.0	0.59591	0.59597

method, is presented in Table 1. Under conditions where there is no internal heat generation and the thermal heat conductivity of the extended surface is constant, it is observed that increasing the thermo-geometric, magnetic field, and porosity parameters results in a decrease in the fin efficiency rate. It was also found that variable thermal conductivity enhances the efficiency of the extended surface. This result suggests that if a fin is designed with the ability to adjust its thermal conductivity in response to changing conditions dynamically, it can improve its heat transfer performance. This underscores the importance of material selection and highlights the potential benefits of using materials with adaptable thermal properties in heat transfer applications. However, the efficiency of the extended surface is suppressed in designs characterized by an apparent increase in heat. This implies that factors such as elevated ambient temperature or enhanced heat transfer rates negatively impact the efficiency of the extended surface.

Table 1 also validates the accuracy and reliability of the methodology used in this study. A comparative analysis shows that the outputs generated by the neural network closely align with those derived through the spectral-based method. The deviation between the two sets of outputs remains within 10^{-4}, underscoring the relatively high degree of precision exhibited by the DNN outputs. This result highlights the robustness and efficacy of the DNN in producing solutions consistent with those obtained through established traditional numerical methods such as spectral methods. By demonstrating its ability to closely replicate the results of conventional numerical methods, the neural network technique establishes itself as a reliable predictive modelling and analysis tool. This validation not only bolsters confidence in the methodology adopted for this study but also underscores the potential of neural network-based approaches in various scientific and engineering applications. Its ability to accurately capture complex relationships and patterns makes this approach valuable for scientific research, particularly in seeking efficient and reliable solutions to a wide range of differential models.

5 Concluding remarks

The primary objective of this study is to develop a deep learning algorithm for approximating the solution of a differential equation that describes the intricate dynamics of heat transfer on extended surfaces. The study also seeks to elucidate the physical implications of some physical parameters arising from the differential model. A DNN architecture was designed to approximate the solution of the nonlinear differential model to achieve these objectives. In order to measure the accuracy and reliability of the neural network technique, a spectral-based numerical method was used to benchmark the result of the neural network technique. The results obtained were accurate, validating the efficiency of the proposed method as a reliable tool for solving and analyzing nonlinear differential models, especially those describing heat transfer in extended surfaces. The finding of this study provides several key insights regarding the thermal behaviour of extended surfaces. Notably, it was observed that variations in the thermal radiation parameter exert a comparable influence on reducing the fin temperature at the tip when compared to changes in the internal heat generation parameters. The study further showed that using materials with varying thermal conductivity can enhance the efficiency of an extended surface, thus optimizing the heat transfer process. Overall, these findings are significant in designing, managing and optimizing extended surfaces.

Acknowledgments: The authors wish to acknowledge the critical review provided by the anonymous reviewers which improved the quality and clarity of this article.

Funding information: This work was based on the research supported in part by the National Research Foundation of South Africa (Ref Number: TTK2204163593). Yusuf Olatunji Tijani acknowledges the support of Rhodes University.

Author contributions: Shina D. Oloniiju: conceptualization, investigation, methodology, software, writing – original draft, reviewing and editing, supervision. Yusuf O. Tijani: conceptualization, investigation, methodology, writing – original draft, reviewing and editing. Olumuyiwa Otegbeye – conceptualization, methodology, writing – original draft, reviewing and editing, supervision. All authors have accepted responsibility for the entire content of this manuscript and approved its submission.

Conflict of interest: The authors state no conflict of interest.

Data availability statement: Data sharing is not applicable to this article as no datasets were generated or analyzed during the current study.

References

[1] Madhura KR, Babitha, Kalpana G, Makinde OD. Thermal performance of straight porous fin with variable thermal conductivity

under magnetic field and radiation effects. Heat Transfer. 2020;49(8):5002–19.
[2] Gorla RSR, Bakier AY. Thermal analysis of natural convection and radiation in porous fins. Int Commun Heat Mass Transfer. 2011;38(5):638–45.
[3] Kiwan S, Al-Nimr M. Enhancement of heat transfer using porous finns. ASME J Heat Transfer. 2001;123(4):790–5.
[4] Hatami M, Ganji DD. Thermal behavior of longitudinal convective-radiative porous fins with different section shapes and ceramic materials (SiC and Si3N4). Ceramics Int. 2014;40:6765–75.
[5] Gireesha BJ, Keerhi ML, Sowmya G. Effects of stretching/shrinking on the thermal performance of a fully wetted convective-radiative longitudinal fin of exponential profile. Appl Math Mechanics. 2022;43:389–402.
[6] Atouei SA, Hosseinzadeh Kh, Hatami M, Sahebi SAR, Ghasemi SE, Ganji DD. Heat transfer study on convective-radiative semi-spherical fins with temperature-dependent properties and heat generation using efficient computational methods. Appl Therm Eng. 2015;89:299–305.
[7] Nicholls RA, MoghimI MA, Griffiths AL. Impact of fin type and orientation on performance of phase change material-based double pipe thermal energy storage. J Energy Storage. 2022;50:104671.
[8] Aziz A, Lopez RJ. Convection-radiation from a continuously moving, variable thermal conductivity sheet or rod undergoing thermal processing. Int J Therm Sci. 2011;50:1523–31.
[9] Razani A, Ahmadi G. On optimization of circular fins with heat generation. J Franklin Inst. 1977;303(2):211–8.
[10] Buonomo B, Cascetta F, Manca O, Sheremet M. Heat transfer analysis of rectangular porous fins in local thermal non-equilibrium model. Appl Therm Eng. 2021;195:117237.
[11] Aderogba AA, Fabelurin OO, Akindeinde SO, Adewumi AO, Ogundare BS. Nonstandard finite difference approximation for a generalized fins problem. Math Comput Simul. 2020;178:183–91.
[12] Sowmya G, Thanesh-Kumar K, Srilatha P, Varun-Kumar RS, Madhu J. Performance analysis of a longitudinal fin under the influence of magnetic field using differential transform method with Pade approximant. ZAMM J Appl Math Mech. 2022;102(11):e202100464.
[13] Kasali KB, Akindeinde SO, Tijani YO, Adewumi AO, Lebelo RS. Thermal and multi-boiling analysis of a rectangular porous fin: A spectral approach. Nonl Eng. 2022;11(1):654–63.
[14] Motsa SS. A new spectral local linearization method for nonlinear boundary layer flow problems. J Appl Math. 2013;013:423628.
[15] Akindeinde SO. Parker-Sochacki method for the solution of convective straight fins problem with temperature-dependent thermal conductivity. Int J Nonl Sci. 2018;25(2):119–28.
[16] Sobamowo GM. Combined impacts of fin surface inclination and magnetohydrodynamics on the thermal performance of a convective-radiative porous fin. J Appl Comput Mech. 2022;8(3):940–8.
[17] Zhanga C, Li X. Temperature distribution of conductive-convective-radiative fins with temperature-dependent thermal conductivity. Int Commun Heat Mass Transfer. 2020;117:104799.
[18] Roy PK, Mallick A, Mondal H, Sibanda P. A modified decomposition solution of triangular moving fin with multiple variable thermal properties. Arabian J Sci Eng. 2018;43(2):1485–97.
[19] Lagaris IE, Likas A, Fotiadis DI. Artificial neural networks for solving ordinary and partial differential equations. IEEE Trans Neural Netw Learn Syst. 1998;9(5):987–1000.
[20] Waseem W, Sulaiman M, Islam S, Kumam P, Nawaz R, Raja MAZ, et al. A study of changes in temperature profile of porous fin model using cuckoo search algorithm. Alexandr Eng J. 2020;59(1):11–24.
[21] Tan CK, Ward J, Wilcox SJ, Payne R. Artificial neural network modelling of the thermal performance of a compact heat exchanger. Appl Thermal Eng. 2009;29(17–18):3609–17.
[22] Goud JS, Srilatha P, Kumar RSV, Sowmya G, Gamaoun F, Nagaraja KV, et al. Heat transfer analysis in a longitudinal porous trapezoidal fin by non-Fourier heat conduction model: An application of artificial neural network with Levenberg-Marquardt approach. Case Stud Therm Eng. 2023;49:103265.
[23] Kumar RSV, Alsulami MD, Sarris IE, Sowmya G, Gamaoun F. Stochastic Levenberg-Marquardt neural network implementation for analyzing the convective heat transfer in a wavy fin. Mathematics. 2023;11(10):3609–17.
[24] Shafiq A, Çolak AB, Sindhu TN. Development of an intelligent computing system using neural networks for modeling bioconvection flow of second-grade nanofluid with gyrotactic microorganisms. Numerical Heat Transfer, Part B: Fundamentals; 2023. p. 1–18.
[25] Shafiq A, Çolak AB, Sindhu TN, Lone SA, Alsubie A, Jarad F. Comparative study of artificial neural network versus parametric method in COVID-19 data analysis. Results Phys. 2022;38(5):105613.
[26] Shafiq A, Çolak AB, Sindhu TN. Modeling of Soret and Dufour's convective heat transfer in nanofluid flow through a moving needle with artificial neural network. Arabian J Sci Eng. 2022;48(5):2807–20.
[27] Sobamowo GM, Kamiyo OM. Multi-boiling heat transfer analysis of a convective straight fin with temperature-dependent thermal properties and internal heat generation. J Appl Comput Mechanics. 2017;3(4):229–39.
[28] Liu I. On Fourier's law of heat conduction. Contin Mech Thermodyn. 1990;2(4):301–5.
[29] Singha S, Kumara D, Rai KN. Wavelet collocation solution of nonlinear fin problem with temperature dependent thermal conductivity and heat transfer coefficient. Int J Nonl Anal Appl. 2015;1(6):105–18.
[30] Oguntala GA, Abd-Alhameed R. Haar wavelet collocation method for thermal analysis of porous fin with temperature-dependent thermal conductivity and internal heat generation. J Appl Comput Mech. 2017;3(3):185–91.
[31] Sobamowo MG, Oguntala GA, Yinusa AA. Nonlinear transient thermal modeling and analysis of a convective-radiative fin with functionally graded material in a magnetic environment. Model Simul Eng. 2019;2:1–16.
[32] Trefethen LN. Spectral methods in MATLAB. Philadelphia: SIAM; 2000.